Emergent Materials
https://doi.org/10.1007/s42247-024-00896-7

ORIGINAL ARTICLE

Novel insights into PLMN-13PT ceramics: impact of spark plasma sintering on compositional and dielectric properties

Fernando Londoño[1] · William Junior do Nascimento[2] · Diego Seiti Fukano Viana[3] · Jose Antonio Eiras[3] · Ducinei Garcia[3]

Received: 9 August 2024 / Accepted: 2 October 2024

Abstract
This study investigates the effects of Spark Plasma Sintering (SPS) on the physical, structural, microstructural, dielectric, and optical properties of on 87[$Pb_{(1-y)}La_x(Mg_{1/3}Nb_{2/3})O_3$]-13$PbTiO_3$, (PLMN-13PT) ceramics. The primary objective was to evaluate how SPS influences the densification, grain growth, and compositional variations of these ceramics, which are critical for electronic device applications. The results demonstrate that SPS effectively achieves high relative density while suppressing grain growth, leading to a more homogeneous microstructure. However, the rapid densification process also induces compositional variations that significantly impact the dielectric properties, including the reduction of undesirable phases like pyrochlore, which are detrimental to performance. These findings highlight the potential of SPS for optimizing PLMN-13PT ceramics, enhancing their suitability for the miniaturization of multifunctional electronic devices.

Keywords Ceramic · Spark plasma sintering · Dielectric · Microstructure · Structure

1 Introduction

Spark Plasma Sintering (SPS) is an advanced sintering technique used to consolidate powders into dense materials. The process involves applying a pulsed electric current directly to the powder while simultaneously applying pressure. This method enhances the densification process by generating heat both within the particles and at their surfaces, reducing sintering times and temperatures compared to conventional sintering techniques. SPS is particularly beneficial for materials that are difficult to sinter, such as ceramics and composites, as it helps maintain fine grain structures and uniform microstructures, leading to improved mechanical properties [1, 2]. Besides, with this technique, the materials' electrical, mechanical, and thermal properties are remarkably improved [3]. In the same way, SPS offers significant advantages over conventional sintering by allowing precise control over grain growth through its rapid heating rates and shorter sintering times, resulting in finer grain structures that enhance mechanical and physical properties. In contrast, conventional sintering, with its longer heating periods, often leads to coarser microstructures. Additionally, SPS produces more uniform microstructures with fewer defects, such as porosity and grain boundary impurities, due to the electric field and pulsed current aiding densification, whereas conventional sintering can result in non-uniform grain sizes and residual porosity, negatively affecting material properties [1, 3].

Perovskite materials are critical to the electro-electronic industry due to their exceptional properties. Organo-inorganic metal halide perovskites, for instance, exhibit low exciton binding energy, ambipolar charge transport, and long-range carrier mobility, alongside the advantage of facile solution processing. These characteristics make them highly suitable for the development of high-performance solar cells, with power conversion efficiencies (PCE) reaching up to 26.1% [4, 5]. Furthermore, the perovskite structure is predominant in many ferroelectric, piezoelectric, and dielectric ceramics, which are essential for various electro-electronic applications [6]. Alike, titanium-based ceramics,

✉ Fernando Londoño
falondonob@gmail.com

1 Universidad de Antioquia, Medellín, Colombia

2 Universidade Federal do Paraná, Campus Jandaia do Sul, Curitiba, Brasil

3 Grupo de materiais ferroicos, Universidade Federal de São Carlos, Rod. Washington Luiz, km 235, 13565-905 São Carlos, SP, Brasil

Published online: 31 October 2024

particularly pyrochlores such as $A_2Ti_2O_7$, are increasingly recognized for their crucial role in advanced technological applications due to their unique combination of electrical, thermal and chemical properties. These materials exhibit high ionic conductivity, low activation energy and excellent chemical stability, making them suitable for use in electronic devices and solid oxide fuel cells [7]; however, when they occur as second phases in lead-based ceramics, the dielectric properties of such ceramics are affected [8].

Lead niobate-magnesium-lead titanate (PMN-PT) ceramics have emerged as a focal point in the study of transparent electro-optic materials, owing to their superior electro-optic properties and transparency across both the visible and near-infrared spectra. These ceramics exhibit a high electro-optic coefficient, which significantly enhances device performance by enabling rapid switching and reduced power consumption [9]. The successful synthesis of solid-solution relaxor ferroelectric single crystals, such as PMN-PT, represents a significant advancement in ferroelectric materials research, as these crystals exhibit piezoelectric coefficients that surpass those of conventional materials [10]. Current research efforts are concentrated on further optimizing these properties, particularly for applications in high-frequency medical transducer arrays and ultralow field-driven actuators. The incorporation of local structural heterogeneity, particularly via A-site modification, has demonstrated substantial potential in enhancing the piezoelectric performance of PMN-PT ceramics. For instance, A-site doping with lanthanum has yielded ceramics with elevated dielectric constants and electro-optic coefficients, especially in the PLMN-13PT composition [8]. These attributes position PMN-PT ceramics as a critical material for the advancement of next-generation electro-optic and piezoelectric devices.

On the other way, the advancement in technology and the miniaturization of the electronic industry have led to the need for new materials with enhanced properties. In the development of materials this can be achieved through material doping or by altering the material production processes [11]. Some of these materials can be defined as smart or multifunctional materials, capable of changing their mechanical or physical properties in response to a specific stimulus [12]. In the case of ferroelectric materials such as lanthanum modified lead zirconate titanate, (PLZT), lanthanum-modified lead titanate, (PLT), and lead magnesium niobate-lead titanate, (PMN-PT), numerous studies demonstrate that these materials can be doped with rare earth elements, like in the PLZT and PMN-PT systems. These materials exhibit photoluminescent properties in addition to their inherent electrical, optical, electro-optical, ferroelectric, and dielectric characteristics, making them ideal for the development of multifunctional devices [13]. For example, research on incorporating rare earth elements into the PMN-PT system has demonstrated significant enhancements in the material's properties. Notably, these studies have revealed that PMN-PT ceramics exhibit high electro-optic coefficients, along with excellent dielectric and photoluminescent characteristics. These advanced properties make PMN-PT an attractive option for the development of multifunctional devices, offering potential applications in areas such as optoelectronics and advanced sensors [14–16].

The miniaturization of electronic devices has underscored the importance of controlling grain size in ceramic materials, as smaller grains can enhance both electrical and mechanical properties, which are crucial for developing more compact and efficient components [17],. In this context, understanding the relationship between grain size and the properties of PLMN-13PT ceramics is essential, particularly with regard to the effects of the densification process, including factors such as temperature, time, pressure, and compositional variation. Compositional variation has been identified as a key factor influencing the sintering process, affecting not only the grain growth but also the uniformity and overall densification of the material. Despite the recognized importance of these factors, limited information exists on the impact of Spark Plasma Sintering (SPS) on the densification of the PLMN-13PT system. This study, therefore, explores for the first time the effects of SPS on the structural, microstructural, and electro-electronic properties of PLMN-13PT ceramics, with a particular focus on how compositional variation drives the sintering behavior. The findings are expected to provide new insights into optimizing material performance and fabrication techniques, significantly advancing the development of miniaturized multifunctional devices in the electronics industry.

2 Experimental procedure

In this study, the solid-state method was chosen for its simplicity, requiring only solid reagents, a furnace, and grinding equipment, making it both accessible and straightforward to implement in research and industrial settings [18]. The starting materials used were lanthanum oxide (La_2O_3, $>99\%$ purity), niobium oxide (Nb_2O_5, 99.9+% purity), magnesium carbonate hydroxide pentahydrate ($(MgCO_3)_4{\cdot}Mg(OH)_2{\cdot}5\,H_2O$, 99% purity), lead oxide (PbO, 99% purity), and titanium oxide (TiO_2, 99.8% purity) powders. These powders were synthesized using the columbite method (the combination of the solid-state and columbite methods effectively reduces or eliminates secondary phases in lead-based systems, ensuring high material quality [19]) to prepare $87[Pb_{(1-y)}La_x(Mg_{1/3}Nb_{2/3})O_3]$-$13PbTiO_3$ (PLMN-13PT), with $y=0.01$. The resultant powder was

then calcined at 900 °C for 4 h in an oxygen atmosphere [20].

The densification process was conducted using spark plasma sintering, wherein the powder was placed in a graphite die with a diameter of 5 mm. The heating rate was set at 100 °C/min, ramping from room temperature to 900 °C, where it remained for 10 min. The entire process was performed under vacuum with a sintering pressure of 29 MPa in an SPS apparatus (SPS-515 S, SCM, Izumi Tech. Co. Ltd., Tokyo, Japan). This pressure value was selected after multiple tests at various pressures, as it proved suitable for achieving a crack-free ceramic material with high density. The spark plasma-sintered bodies were reoxidized by heat treatment at 900 °C for 1 h in an oxygen atmosphere, using double crucibles to minimize the volatilization of lead oxide and maintain a PbO-rich atmosphere. The reoxidation process was implemented to restore the yellow color and characteristic transparency typical of ceramics obtained from lead-based materials [21, 22]. This process reduces or eliminates the oxygen vacancies formed during spark plasma sintering, which result from the argon atmosphere used, as noted by Reimann et al. in their studies on KNN piezoelectric systems. The reduction of oxygen vacancies is crucial for enhancing the electrical properties and stability of ceramic materials because oxygen vacancies tend to accumulate at grain boundaries. These vacancies can act as charge traps, disrupting the local electric field and hindering the polarization of the material [23].

The density of the samples was measured using the Archimedes method, with a system adapted to a Sartorius Micronal balance, model B582. X-ray diffraction (XRD) analysis was performed using a Rigaku diffractometer with CuKα radiation to determine the phases and structural parameters. Measurements were carried out at room temperature, and lattice parameters were calculated using the least squares method based on the positions of the diffraction peaks. Refinement of the lattice parameters was achieved using the DBWS9807 program. The microstructural features of the samples were examined through scanning electron microscopy (SEM) using a Jeol JSM 5800 LV. Grain sizes were determined from the surface SEM images using the linear-intercept method. Dielectric measurements as a function of temperature and frequency were conducted via impedance analysis (HP4194A). Finally, the optical transmittance as a function of wavelength was measured using a spectrophotometer (Micronal, model B582).

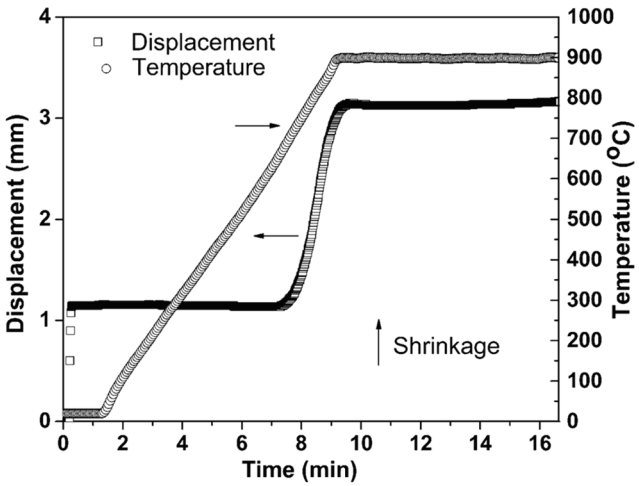

Fig. 1 Temperature and shrinkage behavior over time during SPS sintering of PLMN-13PT powder

3 Results and discussion

3.1 Analysis of dimensional shrinkage and temperature variations during spark plasma sintering

Figure 1 illustrates the shrinkage and temperature changes during the Spark Plasma Sintering (SPS) densification of PLMN-13PT powder over time. The powder exhibits a shrinkage of 2 mm, corresponding to approximately 40% shrinkage, consistent with results observed by Nascimento et al. for PFW system powders [24]. Nascimento highlights the significant contribution of the SPS system to shrinkage, which can be seen in the decrease of shrinkage during the cooling process. Based on the density measurement of 99% obtained through the Archimedes method, the actual shrinkage of the system is estimated to be around 25% [25]. SPS densification generally results in higher density measurements compared to conventional processes [26].

For PMN-PT, conventional pressing yields density values around 98%, while SPS sintering results in density measurements exceeding 99%. However, it is possible that the heating rates were too rapid, causing the system to densify quickly, which in turn could prevent the exclusion of micropores. The instruments used in this study may not be capable of detecting these micropores.

Examining the graph in Fig. 1, the compacts show the onset of shrinkage at approximately 300 °C, followed by a rapid increase in shrinkage as temperature increases, until full compaction is reached at around 800 °C. According to the experimental procedure, the temperature increase rate is 100 degrees per minute. This high rate of increase may contribute to the formation of second phases in densified ceramics, which is significantly higher compared to the rates reported for other densification methods applied to this material [27, 28]. A contraction of 2 mm starting at 700 °C and ending at 900 °C is also observed. The densification temperature for ceramics using the conventional state method is known to be 1260 °C [29]. The difference of

almost 400 °C between the two techniques is to be expected, given that SPS activates the surfaces of the particles with high electrical discharges, promoting the transfer of material and resulting in a rapid densification process [24].

Recent studies have shown that the rapid heating rates employed in SPS can lead to enhanced grain growth control and reduced grain boundary diffusion, contributing to the improved mechanical properties of the densified materials. Moreover, the electric field applied during SPS can enhance diffusion rates and reduce the activation energy for sintering, further explaining the lower densification temperatures required for SPS compared to conventional sintering methods. The densification temperature and time are lower compared to values reported by other techniques, which results in limited grain growth, making SPS a suitable technique for obtaining miniaturized multifunctional materials. However, the short densification time could lead to compositional variations within the materials, potentially affecting their electrical properties.

3.2 Microstructural characterization

Figure 2 displays SEM micrographs of the surface of PLMN-13PT ceramic produced by SPS. The average grain size, calculated using the linear intercept method, is 1.19 ± 0.23 µm. This size is significantly smaller than the grain sizes reported for other densification methods used for this system, such as conventional sintering (CS) and hot pressing (HP) [20, 29]. As indicated in several studies, densification by SPS suppresses grain growth due to the short densification time and low densification temperature [24]. Likewise, ceramics obtained by SPS are more homogeneous than those produced by hot pressing or conventional methods, as evidenced not only visually [17] but also by the lower standard deviations in grain size data (Table 1). The phase contours observed are thick and predominantly constituted by the liquid phase of the material. This observation may further indicate the presence of secondary phases in the X-ray diffraction patterns.

3.3 Structural characterization

Figure 3 presents the room temperature X-ray diffraction patterns of the PLMN-13PT powder obtained by spark plasma sintering. The patterns predominantly display peaks corresponding to the perovskite structure with space group P4mm (JCPDS 39-1488). Additionally, a secondary phase related to the pyrochlore structure, $Pb_{1.83}Nb_{1.71}Mg_{0.29}O_{6.39}$ (JCPDS 33–0769), is also observed. The relative amount of the pyrochlore phase was calculated using Eq. (1), based on the maximum intensities of the perovskite and pyrochlore phases in the diffraction pattern shown in Fig. 3. The

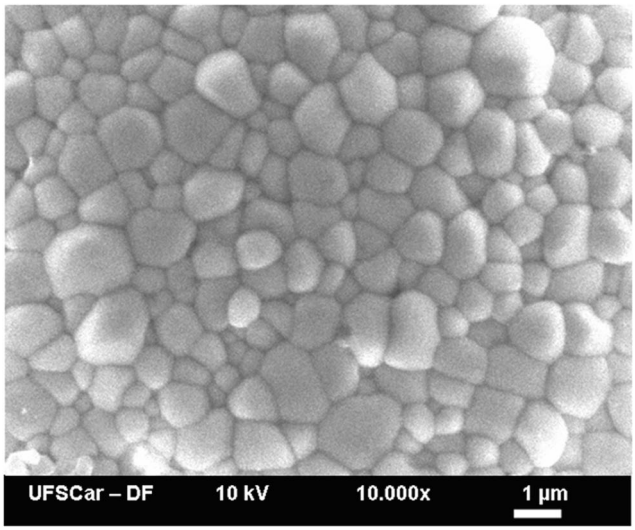

Fig. 2 SEM micrograph of fracture surfaces on PLMN-13PT ceramic obtained by SPS

Table 1 Structural and microstructural properties of PLMN-13PT densified by SPS and CS

	PLMN-13PT CS	PLMN-13PT SPS
Grain size (µm)	8.54±0.56	1.19±0.23
Lattice parameters (Å)		
a	4.012	4.033* ±0.004
c	4.012	4.034*±0.004
c/a	1	~1*
Relative density (%)	96	99

*Pseudo-cubic behavior is observed in the sample

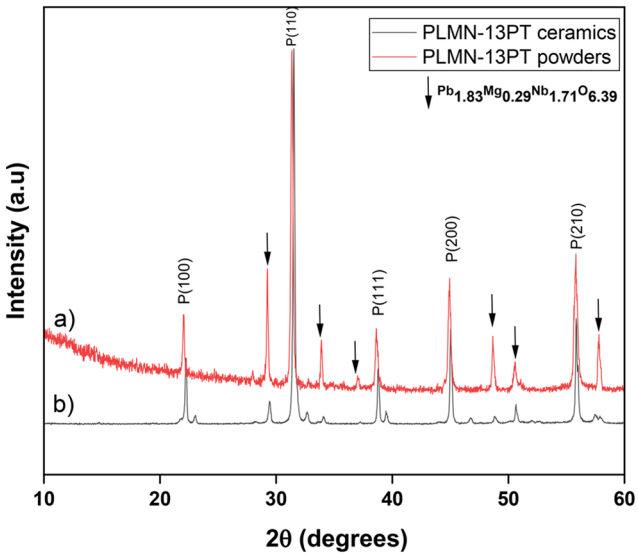

Fig. 3 Room temperature X-ray diffraction patterns of PLMN-13PT a) powders obtained by grinding [20], b) ceramics obtained by spark plasma sintering (heating rate 100°C/min from room temperature to 900°C, for 10 min and sintering pressure of 29 MPa)

pyrochlore phase constituted approximately 27% of the powder and about 5% of the ceramic sample.

$$\%Phase\ Pyrochlore = \frac{I_{pyrochlore}}{I_{pyrochlore} + I_{P(110)}} \quad (1)$$

The results show a marked decrease in the pyrochlore phase after densification, aligning with findings from prior studies [30]. Nevertheless, in this work, it was determined that the persistence of the pyrochlore phase is possibly due to the stages the ceramic undergoes during the densification process: loss of oxygen when using a reducing atmosphere and loss of lead during the heat treatment. Similarly, the high heating rates and simultaneous application of pressure in Spark Plasma Sintering (SPS) may stimulate volumetric transport mechanisms, including grain boundary and volumetric diffusion, facilitating shrinkage and densification [24]. However, we believe that these diffusion processes, combined with the very rapid cooling, lead to increased compositional variations in small regions of the ceramic, which can contribute to the formation of the pyrochlore phase.

Table 1 summarizes the structural and microstructural properties of PLMN-13PT samples prepared using conventional sintering (CS) and spark plasma sintering (SPS) [20, 21]. SPS processing yielded significantly finer grain sizes compared to CS, suggesting superior grain growth control due to the rapid densification process and lower temperatures. While SPS samples exhibited slight lattice expansion or distortion, as indicated by increased a and c parameters, the relationship between them remained constant, indicating that the Goldschmidt tolerance parameter was not affected by the densification process. This suggests that while the SPS process does not alter the fundamental lattice structure of the material, it significantly impacts the formation of secondary phases, density, and microstructural properties. SPS samples attained a markedly higher relative density (99% vs. 96%) than CS counterparts. These microstructural refinements through SPS potentially enhance mechanical properties and improve functional performance due to the finer grain structure. The subtle lattice variations observed may influence material properties and warrant further investigation. Overall, SPS demonstrates clear advantages over CS in terms of microstructural control and densification efficiency.

3.4 Dielectric characterization

Figure 4 displays the results of the study on the real and imaginary permittivity in relation to temperature (150–400 K) and frequency (1 kHz, 10 kHz, 100 kHz and 1 MHz).

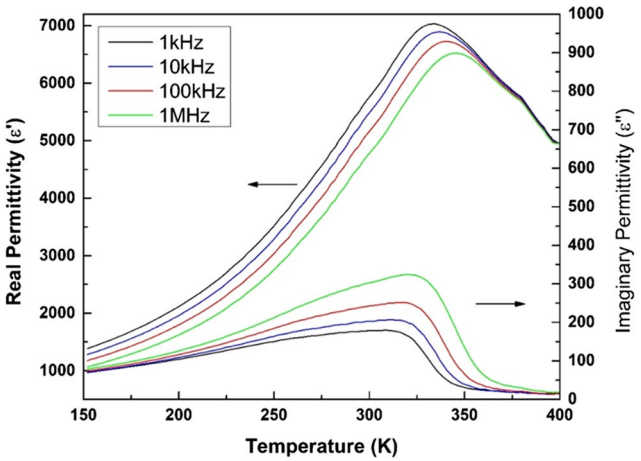

Fig. 4 Real and imaginary permittivity versus temperature at 1 kHz, 10 kHz, 100 kHz and 1 MHz for the PLMN-13PT ceramic system obtained from SPS

Table 2 Dielectric properties from Santos- Eiras equation of PLMN-13PT SPS and PLMN-13PT CS at 1 kHz

Ceramics	ε_{max}	T_{max} (K)	Δ	ξ
PLMN-13PT SPS	7028 ± 1	332.8 ± 0.1	115 ± 1	1.61 ± 0.02
PLMN-13PT CS[20]	25,200	305	45.5 ± 0.03	1.63

The data reveals a diffuse phase transition, as evidenced by a decrease in the maximum real permittivity with increasing frequency and an increase in the temperature at which the maximum occurs (Tm) with increasing frequency. These findings are consistent with the typical behavior of relaxor materials [31].

Table 2 presents the dielectric properties of PLMN-13PT SPS compared to PLMN-13PT CS [20], to 1 kHz, which were calculated using the Santos-Eiras equation [31], where $\boldsymbol{\varepsilon_{max}}$ is the maximum dielectric permittivity and $\mathbf{T_{max}}$ its related temperature. In Table 2, ξ characterizes the phase transition: ξ = 1 indicates a normal ferroelectric transition, ξ = 2 represents a complete diffuse phase transition (DPT) per the Kirilov–Isupov approximation [32], and ξ between 1 and 2 indicates an incomplete DPT, considering ferroelectric cluster interactions [31]. Additionally, Δ is an empirical parameter indicating the DPT degree, related to dielectric permittivity peak broadening.

It is evident that SPS densified samples have a lower dielectric constant value than CS ceramics. Among the various factors that influence the behavior of dielectric constant, the reduction in grain size has a significant impact on lead-based ceramic materials [20]. This is because decreasing the grain size increases the number of grain boundaries, which hinder polarization processes within the material. Besides, the reduction in grain size due to SPS increases the number of grain boundaries, which enhances the dielectric loss due to the buildup of space charges. When electronic space charges are trapped at grain boundaries or other non-homogeneous

regions within the material, they can lead to localized electric fields. These fields cause additional energy dissipation because the trapped charges cannot follow the rapidly alternating external electric field efficiently. As a result, dielectric loss increases. Grain boundaries disrupt the alignment of dipoles and reduce the material's ability to store electrical energy, which is reflected in a lower dielectric permittivity [27]. In addition to grain size reduction, the high diffusivity value (Δ) shown in Table 2 can contribute to variations in the dielectric constant. The increase in diffusivity is known to correlate with compositional variations in the ceramic material [32], likely enhanced by the SPS densification method. Similarly, the increase in T_{max} can also be attributed to compositional variations, as confirmed by the diffusivity value, which aligns with the rapid densification process facilitated by SPS [33]. Besides, non-uniform dielectric constants, generated by compositional variations can lead to localized electric field variations, impacting the overall performance of the material in practical applications. This is significant because the dielectric constant directly affects the material's ability to store electrical energy, impacting its suitability for electronic devices.

As noted earlier, heat treatment likely caused lead volatilization from the A-sites in the perovskite structure, leading to the formation of Pb vacancies. This reduction in internal stress after annealing plays a crucial role in weakening the relaxation state and decreasing the dielectric constant [34]. Additionally, the higher diffusion values observed in SPS-densified ceramics are linked to residual pyrochlore-type secondary phases, which may also have formed due to lead volatilization.

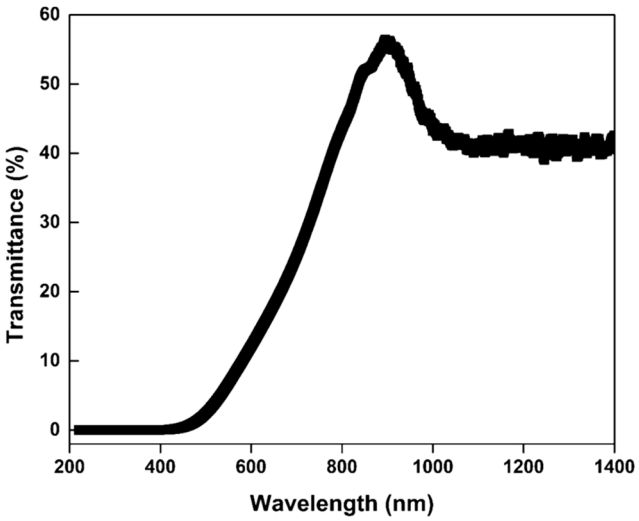

Fig. 5 Transmittance as a function of wavelength of incident light for optically polished PLMN-13PT ceramic with a thickness of 500 μm

3.5 Transmittance characterization

The Fig. 5 shows the transmittance percentage of a material as a function of wavelength, ranging from 200 nm to 1400 nm, covering the ultraviolet (UV), visible, and near-infrared (NIR) regions. The transmittance percentage ranges from 0 to 60%, indicating how much light passes through the material. From 200 nm to around 600 nm, transmittance is low, suggesting strong absorption in the UV to early visible spectrum, this behavior is typical of lead-based ceramics with perovskite-type structure [35]. There is a sharp increase in transmittance starting around 600 nm, peaking slightly above 50% at approximately 850 nm, indicating greater transparency in the visible to NIR transition. After this peak, transmittance slightly decreases and then stabilizes just below 50% in the NIR region. The low UV transmittance suggests strong absorption due to electronic transitions, while the increased transmittance in the visible to NIR region indicates suitability for applications in NIR photodetectors that used in applications such as remote sensing, night vision, and medical imaging [36]. Finally, the material could be used in optical filters too, sensors, or coatings needing selective transmittance in the visible to NIR regions, and its sharp increase and plateau suggest potential use in photonic devices [37].

Compared to results achieved by other densification processes using the same system, our transmittance measurements exhibit lower values. This difference may be attributed to the smaller grain sizes observed in our ceramics, which contain a higher percentage of grain boundaries. These boundaries serve as light scattering centers, reducing the overall transmittance percentage of the ceramics. Similarly, in materials with smaller grains, the limited space within individual grains restricts the expansion of ferroelectric domains, leading to an increased number of domain walls. These domain walls can also act as centers for light scattering, further affecting the material's optical properties. Besides, the increase in transmittance between 500 nm and 900 nm for the sample obtained by SPS has a lower slope than the increase in transmittance of PLMN-PT ceramics obtained by other densification methods. We attribute this to the generation of micropores and small grains during the quick sintering process that produces Rayleigh scattering [38]. Besides, although a peak between 800 and 900 nm was observed, the underlying causes for its occurrence remain inconclusive. Further studies will be needed to establish the factors that contribute to this peak and to fully understand its origin.

4 Conclusion

In this work, we successfully obtained ceramics with high density, homogeneous grain size, and a high proportion of the desired phase, making them suitable for multifunctional device applications. The Spark Plasma Sintering (SPS) process significantly impacts the structural and microstructural properties of PLMN-13PT ceramics by inhibiting grain growth and inducing compositional variations, which in turn affect the dielectric properties. Specifically, SPS processing achieved a relative density of 99%, with grain sizes reduced to 1.19 ± 0.23 µm, compared to 8.54 ± 0.56 µm for conventional sintering. These microstructural refinements enhance the mechanical and functional properties of the ceramics, making them ideal for miniaturized electronic devices, sensors, and photonic applications. However, the rapid heating and cooling rates in SPS can lead to significant compositional inhomogeneities, such as uneven element distribution and phase formation, which can adversely affect the dielectric and structural properties of PLMN-13PT ceramics. While conventional sintering provides more stable compositions, it does not offer the same level of microstructural control. To fully capitalize on the benefits of SPS, future research should focus on optimizing the sintering conditions to minimize compositional variations and enhance the overall performance of these ceramics.

Acknowledgements To CAPES, FAPESP, CNPq and -Universidad de Antioquia for the financial support. To Dra. Y.P Masacarenhas (Sao Carlos Physics Institute at the university Sao Paulo), for the use of the XRD laboratory facilities, and to Ms Natalia Zanardi for the technical support.

Funding Open Access funding provided by Colombia Consortium.

References

1. Z.Y. Hu, Z.H. Zhang, X.W. Cheng, F.C. Wang, Y.F. Zhang, S.L. Li, A review of multi-physical fields induced phenomena and effects in spark plasma sintering: Fundamentals and applications. Mater Des [Internet]. **191,** 108662 (2020). https://doi.org/10.1016/j.matdes.2020.108662
2. C.E.J. Dancer, Flash sintering of ceramic materials. Mater. Res. Exp. **3**(10) (2016)
3. S. Supriya, Electric field assisted spark plasma sintering of ABO3 perovskites: Crystal structure, dielectric behavior and future challenges. Open. Ceram. **18** (2024)
4. B. Li, S. Li, J. Gong, X. Wu, Z. Li, D. Gao et al., Fundamental understanding of stability for halide perovskite photovoltaics: The importance of interfaces. Chem [Internet]. **10**(1),35–47 (2024). https://www.sciencedirect.com/science/article/pii/S2451929423004308
5. N. Parikh, M.M. Tavakoli, M. Pandey, M. Kumar, D. Prochowicz, R.D. Chavan et al., Two-dimensional halide perovskite single crystals: principles and promises. 2020. https://doi.org/10.1007/s42247-021-00177-7
6. R. López-Juárez, F. González, M.E. Villafuerte-Castrejón, Lead-Free Ferroelectric Ceramics with Perovskite Structure. In: Lallart M, editor. Ferroelectrics [Internet]. Rijeka: IntechOpen; 2011. p. Ch. 15. https://doi.org/10.5772/20107
7. S. Supriya, *Influence of rare Earth Coordinated Elements in titanium-based Pyrochlores and Their Dielectric Phenomena*, Coordination Chemistry Reviews vol. 493 (Elsevier B.V., 2023)
8. F. Andrés, L. Badillo, J.A. Eiras, P. Milton, D. Garcia, Preparation and Microstructural, Structural, Optical and Electro-Optical properties of La Doped PMN-PT transparent ceramics. Opt. Photonics J. **2**, 157–162 (2012)
9. M. Hu, Y. Wu, L. Chen, W. Dong, Q. Fu, Effects of rare earth dopants on the EO properties and domain configurations in PMN-PT transparent ceramics. J. Mater. Sci.: Mater. Electron. **35**(9) (2024)
10. F. Li, M.J. Cabral, B. Xu, Z. Cheng, E.C. Dickey, J.M. LeBeau et al., Giant piezoelectricity of Sm-doped Pb(Mg 1/3 Nb 2/3)O 3-PbTiO 3 single crystals [Internet]. Available from: https://www.science.org
11. Chu Sheng-Yuan, Doping effects on the dielectric properties of low temperature sintered lead-based ceramics. Mater. Res. Bull. **35**, 1067–1076 (2000)
12. J.K. Guest, J.H. Prévost, Optimizing multifunctional materials: design of microstructures for maximized stiffness and fluid permeability. Int. J. Solids Struct. **43**(22–23), 7028–7047 (2006)
13. L. Stella Arias Maya, I. Mecánico, P. Asistente, MATERIALES COMPUESTOS INTELIGENTES. Scientia Et Technica. **25**, 143–148 (2004)
14. Z. Fang, X. Tian, F. Zheng, X. Jiang, W. Ye, Y. Qin et al., Enhanced piezoelectric properties of Sm3+-modified PMN-PT ceramics and their application in energy harvesting. Ceram. Int. **48**(6), 7550–7556 (2022)
15. A. Hussain, N. Sinha, S. Goel, A.J. Joseph, B. Kumar, Y3 + doped 0.64PMN-0.36PT ceramic for energy scavenging applications: excellent piezo-/ferro-response with the investigations of true-remanent polarization and resistive leakage. J. Alloys Compd. **790**, 274–287 (2019)
16. N. Zhong, P.H. Xiang, D.Z. Sun, X.L. Dong, Effect of rare earth additives on the microstructure and dielectric properties of 0.67Pb(Mg1/3Nb2/3)O3-0. 33PbTiO3 ceramics. Mater. Sci. Eng. B Solid State Mater. Adv. Technol. **116**(2), 140–145 (2005)
17. P. Marchet, B. Malic, M. Deluca, M. Van Bael. Editorial: recent advances and future of electroceramics. Open. Ceram. **10** (2022)
18. S.V.J. V P V, C K S, A M HT, K M N. Profound investigation of photoluminescent characteristics of Li + sensitized BaCeO3:Sm3 + perovskite synthesized through both combustion and solid-state reaction techniques. Emergent Mater. 2024
19. T. Garg, M. Mukesh, L.M. Goyal, K.H. Mir, A systematic investigation to establish a structure-property correlation in 0.65PMN–0.35PT ceramics. J. Mater. Sci. Mater. Electron. **35**(3) (2024)
20. F.A. Londoño, J. Eiras, F.P. Milton, D. Garcia, Preparation and microstructural, structural, optical and electro-optical properties

of la doped Pmn-Pt transparent ceramics. Opt. Photonics J. **02**(03), 157–162 (2012)
21. F.A. Londoño, J.A. Eiras, D. Garcia, Novas cerâmicas ferroelétricas transparentes com. Cerâmica. **57**, 404–408 (2011)
22. Y. Wenhu, P. Yongping, C. Xiaolong, W. Jinfei, Study of reoxidation in heavily La-doped barium titanate ceramics. J. Phys. Conf. Ser. 2009;**152**
23. T. Reimann, S. Fröhlich, A. Bochmann, A. Kynast, M. Töpfer, E. Hennig et al., Low pO2 sintering and reoxidation of lead-free KNNLT piezoceramic laminates. J. Eur. Ceram. Soc. **41**(1), 344–351 (2021)
24. W.J. Do Nascimento, Sinterização De Cerâmicas, Multiferróicas Nanoestruturadas De PbFe 1/2 Nb 1/2)O 3 E Pb(Fe 2/3 W 1/3) O 3 VIA "Spark Plasma Sintering-SPS." [São Carlos] (Universudade Federal de São Carlos, 2013)
25. R.M. German, *Sintering Theory and Practice* (Wiley, New York, 1996)
26. U. Anselmi-Tamburini, J.E. Garay, Z.A. Munir, A. Tacca, F. Maglia, G. Spinolo, Spark plasma sintering and characterization of bulk nanostructured fully stabilized zirconia: part I. densification studies. J. Mater. Res. **19**(11), 3255–3262 (2004)
27. R. Zuo, T. Granzow, D.C. Lupascu, J. Rödel, PMN-PT ceramics prepared by spark plasma sintering. J. Am. Ceram. Soc. **90**(4), 1101–1106 (2007)
28. A. Babapoor, M.S. Asl, Z. Ahmadi, A.S. Namini, Effects of spark plasma sintering temperature on densification, hardness and thermal conductivity of titanium carbide. Ceram. Int. **44**(12), 14541–14546 (2018)
29. F.A. Londoño, A. Herrera, D. Garcia, Efecto de la adición de tierras raras en las propiedades de las cerámicastransparentes PLMN-13PT:RE. Boletin de la Sociedad Espanola de Ceramica y Vidrio. 1–9 (2021)
30. A. Chang, B. Zhang, Y. Wu, Q. Zhao, H. Zhang, J. Yao et al., *Spark Plasma Sintering of Negative Temperature Coefficient Thermistor Ceramics* (Sintering Techniques of Materials, 2015)
31. I.A. Santos, J.A. Eiras, Phenomenological description of the diffuse phase transition in ferroelectrics. J. Phys. Condens. Matter **13** (2001)
32. V.V. Kirillov, V.A. Isupov, Relaxation polarization of pbmg 1/3nb2/303(pmn-a ferroelectric with a diffused phase transition. Ferroelectrics. **5**(1), 3–9 (1973)
33. M. Tokita, Progress of spark plasma sintering (sps) method, systems, ceramics applications and industrialization. Ceramics. **4**(2), 160–198 (2021)
34. Y. Hou, N. Wu, C. Wang, M. Zhu, X. Song, Effect of annealing temperature on dielectric relaxation and raman scattering of 0.65Pb(Mg1/3Nb2/3)O3-0. 35PbTiO3 system. J. Am. Ceram. Soc. **93**(9), 2748–2754 (2010)
35. C. Ding, B. Fang, Q. Du, L. Zhou, Phase structure and electrical properties of 0.8Pb(mg 1/3Nb 2/3)o 3-0.2PbTiO 3 relaxor ferroelectric ceramics prepared by the reaction-sintering method. Phys. Status Solidi (A) Appl. Mater. Sci. **207**(4), 979–985 (2010)
36. Y. Zhang, J. Yun, S. Zhang, L. Zeng, Z. Bi, N. Huang et al., Self-Powered Near-Infrared photodetector based on Graphyne/Hexagonal boron phosphide heterostructure with high responsivity and robustness: a theoretical study. Appl. Surf. Sci. **569** (2021)
37. A. Llordés, G. Garcia, J. Gazquez, D.J. Milliron, Tunable near-infrared and visible-light transmittance in nanocrystal-in-glass composites. Nature. **500**(7462), 323–326 (2013)
38. I.A. Santos, A.L. Zanin, M.H. Lente, S.B. Assis, R. Favaretto, D. Garcia et al., Cerâmicas ferroelétricas transparentes de PLZT e PLMN-PT. Cerâmica. **49**, 92–8 (2003)